Mechatronics 25 (2015) 37–43

Contents lists available at ScienceDirect

Mechatronics

journal homepage: www.elsevier.com/locate/mechatronics

Development of a monolithic compliant SPCA-driven micro-gripper

Dapeng Zhang *, Zhengtao Zhang, Qun Gao, De Xu, Song Liu

Research Center of Precision Sensing and Control, Institute of Automation, Chinese Academy of Sciences, Beijing, China

ARTICLE INFO

Article history:
Received 27 January 2014
Accepted 23 November 2014
Available online 31 December 2014

Keywords:
Micro-gripper
Compliant mechanism
Kinematic model
Static model

ABSTRACT

This paper develops a monolithic compliant SPCA-driven micro-gripper for micro-assembly and describes the mechanism design, kinematic model, static model, control strategy and experimental verification of micro-gripper. The paper includes the following points: (1) the MCM integrates the lever mechanism and parallelogram mechanism so as to magnify the SPCA input and transform the linear input of SPCA into the clamping movement of gripping jaw. In addition, the kinematic model of the MCM is established to describe the relationship between the SPCA input and the output displacement of gripping jaw. (2) The static model of movement jaw is established to analyze the inherent relationship between the gripping force and the strain angle of flexible hinge. (3) The control strategy based on the incremental PID algorithm is applied to control the gripping manipulation of micro-gripper. The control strategy selects the visual or force feedback signal according to the contacting condition between the gripping jaw and clamped micro-object. Finally, a series of experiments were performed to validate the kinematic model, static model and control strategy of micro-gripper. In addition, a glassy micro-tube with 150 μm diameter was clamped non-destructively by the developed micro-gripper.

1. Introduction

It is widely recognized that high precision position systems are required for many applications from micro-assembly to medical instruments, and hence have received increasing attention by many researchers. One of particular interests in this area is the development of robust micro-grippers that can perform many micro-scaled tasks ranging from micro-assembly processes to minimally invasive surgery [1–3]. Micro-gripper is the terminal manipulator contacting the micro-object directly, which can decide the micro-assembly task successful or not. The primary requirement of the micro-gripper in micro-assembly system is to be able to grasp micro-object of different shapes and textures with high accuracy and controlled grasping force [4–6]. This is to ensure that the micro-gripper is able to satisfactorily achieve the goal of grasping without damaging the micro-scaled object which generally would be sensitive to external perturbation and gripping force.

Various types of micro-grippers have been proposed in the literature, such as piezoelectric, electrostatic, magnetic, electro-thermal and shape memory micro-grippers [7–11]. As a typical smart actuator, the stack piezoelectric ceramic actuator (SPCA) has drawn great attention due to several intrinsic advantages such as high force to weight ratio, fast response and high motion resolution [12–14]. Therefore, many researchers developed the SPCA-driven micro-grippers to clamp the micro-object [1–5,15–20]. In the above-mentioned micro-grippers, the monolithic compliant mechanisms (MCM) based on the flexible hinges were generally utilized to amplify the SPCA input and transform the linear input of SPCA into the clamping movement of gripping jaw. The researchers generally design the MCM by FEM, which can simulate the output motion of the MCM under the SPCA pushing. Then according to the simulation results, the designers spent plenty of time in adjusting the geometrical parameters of the MCM repeatedly so as to achieve the expected clamping effect [18,19]. Moreover, the MCM generally adopts the symmetrical structure to clamp the micro-object [5,18–20]. Namely, when SPCA drives the MCM, two gripping jaws symmetrically clamp the micro-object. However, it is difficult that the output displacements of gripping jaws are totally equal due to the fabrication and assembly error of micro-gripper.

The clamped micro-object is generally delicate, so the gripping force between the gripping jaw and micro-object should be measured so as to prevent the micro-object from damaging during the clamping process. At present, there are two methods to detect the gripping force: self-sensing method and affixing strain gauges. Timothy and Yuichi developed the piezoelectric tweezer-type effector with self-sensing capability so that the piezoelectric micro-grippers could be used as a sensor and an actuator simultaneously [21–26]. The piezo-electric self-sensing bridge circuit has

* Corresponding author.
E-mail address: dapeng_zhang80@163.com (D. Zhang).

http://dx.doi.org/10.1016/j.mechatronics.2014.11.006
0957-4158/

been applied to measure the displacement of gripping jaw and gripping force. However, the circuit requires exact capacitive matching of piezoelectric actuator, which has been proven difficult in practice due to the capacitance variation [21,22]. In addition, the self-sensing method was not appropriate for the micro-assembly due to the charge error accumulation during the integration of the current signals. Consequently, very few works refer to the use of self-sensing method for the control of micro-assembly [27]. In addition, some researchers affixed the strain gauges on the flexible hinges of the MCM so that the gripping force was measured by detecting the strain angle of flexible hinge [5,28–30]. However, the inherent relationship between the gripping force and strain angle of flexible hinge has not been discussed.

In the aforementioned micro-grippers, the micro-grippers were controlled by the single feedback signal such as the input force of SPCA, the input displacement of SPCA or the gripping force between the micro-object and gripping jaw [5,31–33]. However, in order to clamp the micro-object rapidly and safely, the control strategy of micro-gripper should select the visual or force feedback signal according to the contacting condition between the gripping jaw and clamped micro-object so that the micro-gripper can provide the micro-object with the desired gripping motion and gripping force.

This paper describes the mechanism design, kinematic model, static model, control strategy and experimental validation of a SPCA-driven micro-gripper. The paper includes the following points: (1) the MCM integrates the lever mechanism and parallelogram mechanism in order to amplify the SPCA input and transform the linear input of SPCA into the clamping movement of gripping jaw. The MCM adopts asymmetric structure to clamp the micro-object so as to improve the gripping accuracy. Moreover, the kinematic model of the MCM is established to describe the relationship between the SPCA input and the output displacement of gripping jaw. According to the kinematic model, the designer can calculate the magnification ratio by the geometrical parameters of MCM so as to avoid modifying the parameters repeatedly. (2) The static model of movement jaw is established to analyze the inherent relationship between the gripping force and strain angle of flexible hinge. According to the static model, the output of gripping force can be adjusted by modifying the geometrical parameters of movement jaw. (3) The control strategy based on the incremental PID is applied to control the clamping manipulation of micro-gripper. The control strategy selects the visual or force feedback signal according to the contacting condition between the gripping jaw and clamped micro-object. Finally, a series of experiments were performed to validate the kinematic model, static model and control strategy. A glassy micro-tube with 150 μm diameter was clamped non-destructively by the developed micro-gripper.

The paper is organized as follows: Section 2 describes the structure and principle of SPCA-driven micro-gripper. Section 3 discusses the kinematic model of the MCM, the static model of movement jaw and control strategy of clamping manipulation. Section 4 focuses on the experiments to validate the established kinematic model, static model and control strategy. Section 5 summarizes the research and suggests the possible directions for the future research.

2. Structure and principle of the SPCA-driven micro-gripper

The 3D model of developed micro-gripper consists of pre-adjustment screw, platform base, SPCA, SPCA cover, MCM and strain sensor, as shown in Fig. 1. The functional description of various components is as follows. I. Pre-adjustment screw: provides the SPCA with preload; II. Platform base: installs the MCM and other units; III. SPCA: provides the MCM with input displacement; IV. SPCA cover: connects the SPCA with platform base; V. MCM: transforms the linear input of SPCA into the clamping motion; VI. Strain sensor: measures the strain angle of flexible hinge.

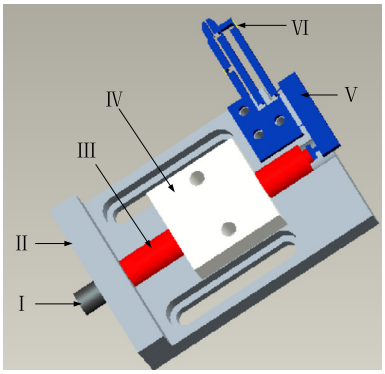

Fig. 1. 3D model of the SPCA-driven micro-gripper.

In general, the MCM is divided into two units: lever mechanism (ABC) and parallelogram mechanism (EFGH), as shown in Fig. 2. The lever mechanism (ABC) is composed of the corner-filleted flexible hinge B, the rigid link AB and BC. When the voltage is applied to the SPCA controller, SPCA drives the MCM at the point A. Then the lever mechanism rotates around the axial center of flexible hinge B, which can amplify the linear input of the SPCA in accordance with the lever principle. The output movement of lever mechanism (ABC) is transmitted to parallelogram mechanism (EFGH) by the rigid link CD. The parallelogram mechanism includes four rigid links: EF, FG, GH and HE. The connecting nodes of adjacent links E, F, G and H adopt the structure of single-notch flexible hinges, as shown in Fig. 2. When the rigid link CD drives the parallelogram mechanism (EFGH), the movement jaw moves toward the stationary jaw due to the rotation of the flexible hinge E, F, G and H around their central axes [21–22]. The parallelogram mechanism is able to further magnify the input motion of rigid link CD by modifying the length of rigid link DE and DF.

3. Modeling and analysis of the micro-gripper

3.1. Kinematic model of the MCM

When establishing the kinematic model of the MCM, we assume that: (1) the flexible hinge is considered as two rigid links and movable hinge with torsion spring; (2) the deformation on the flexure hinge is assumed to be pure rotation without expansion and contraction and the rotational angle is less than 1^0[5]. Therefore, the kinematic model of MCM can be described by several rigid

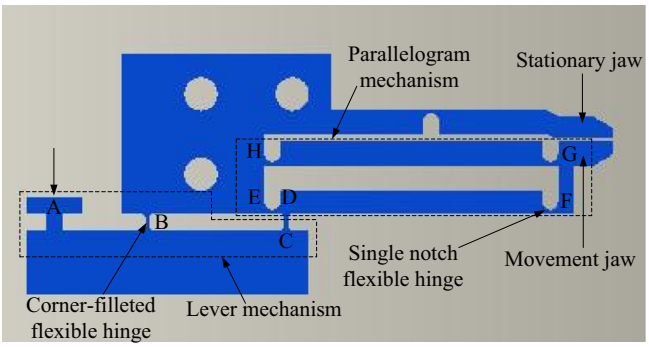

Fig. 2. The structure of developed MCM.

links and flexure hinges $H_1 \sim H_5$, as shown in Fig. 3. Where d_{in} denotes the SPCA input, d_P and d_G indicate the corresponding output of parallelogram mechanism and movement jaw respectively.

When the SPCA pushes the MCM, the flexible hinges $H_1 \sim H_5$ rotate around their central axes so as to achieve the clamping manipulation of the micro-gripper. The solid lines indicate the initial position of the MCM, the dashed lines denote new equilibrium position accordingly, as shown in Fig. 4. The parallelogram mechanism only exhibits one stable equilibrium position due to the small rotational angle of flexible hinges [34,35]. As shown in Fig. 4, the point A denotes the contacting point between the SPCA and MCM. When the SPCA provides the MCM with input displacement d_{in}, the point A moves to A′ due to the rotation of flexible hinge H_1 around the point B (the center of flexible hinge H_1). $\Delta\theta_B$ indicates the rotational angle between the vector AB and A′B. Correspondingly, the endpoint of rigid link CD varies from the point C to C′, the motion distance Δs (point C) can be calculated by the Eq. (1).

$$\Delta s = \frac{(l_2 + l_3)d_{in}}{l_1} \tag{1}$$

When the parallelogram mechanism rotates $\Delta\theta_0$ around the point O (the midpoint of rigid link EH), the corresponding displacement of point C along x and y axis can be calculated by the Eq. (2).

$$\begin{cases} \Delta x_C = x'_C - x_C = |OC|[\sin(\theta_0 + \Delta\theta_0) - \sin\theta_0] = l_4\Delta\theta_0 \\ \Delta y_C = y'_C - y_C = |OC|[\cos(\theta_0 + \Delta\theta_0) - \cos\theta_0] = -l_3\Delta\theta_0 \end{cases} \tag{2}$$

where x_c and y_c denote the initial coordinates of point C, x'_c and y'_c indicate the new equilibrium coordinates. $l_1 \sim l_5$ denote the size of several rigid links. θ_0 indicates the original angle between the vector OC and link HE. $\Delta\theta_0$ denotes the rotational angle due to the position variation of point A, which is generally far less than 1^0. So it can be assumed that: $\cos(\Delta\theta_0) \approx 1$ and $\sin(\Delta\theta_0) \approx 0$.

According to the Eqs. (1) and (2), the SPCA input d_{in} can be indicated by and $l_1 \sim l_5$ and $\Delta\theta_0$, as shown in the Eq. (3). Additionally, according to the geometrical structure of MCM, the output displacement of parallelogram mechanism d_P can be represented by the Eq. (4).

$$d_{in} = \frac{l_1\sqrt{l_3^2 + l_4^2}}{l_2 + l_3}\Delta\theta_0 \tag{3}$$

$$d_P = l_5\Delta\theta_0 \tag{4}$$

Therefore, the theoretical magnification ratio k of MCM can be defined by the Eq. (5).

$$k = \frac{d_P}{d_{in}} = \frac{l_5(l_2 + l_3)}{l_1\sqrt{l_3^2 + l_4^2}} \tag{5}$$

3.2. Static model of the movement jaw

The static model of the movement jaw is established to discuss the inherent relation between the gripping force and the strain angle of flexible hinge H_3. Based on the static model,

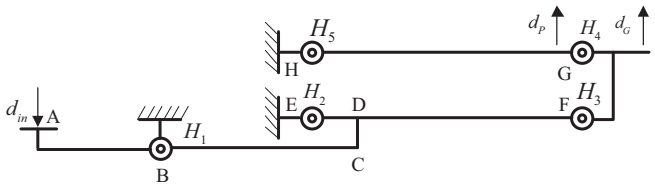

Fig. 3. The kinematic scheme of the MCM.

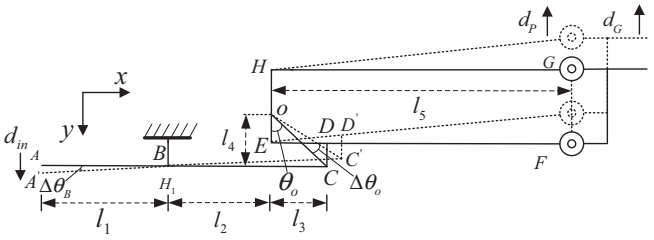

Fig. 4. The kinematic model of the MCM.

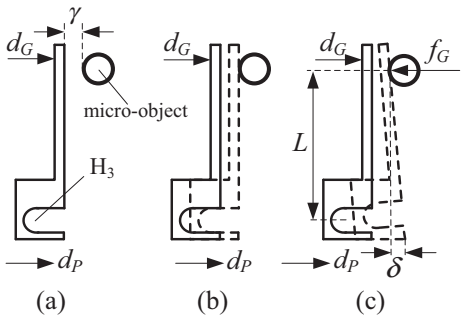

Fig. 5. The grasping process of micro-gripper.

the output of gripping force can be calculated by measuring the strain angle of flexible hinge. Namely, the gripping force of micro-gripper can be regulated by adjusting the geometrical parameters of the movement jaw. The grasping process of micro-gripper can be divided into three stages, as shown in Fig. 5. The movement jaw can be equivalent to cantilever beam, the clamped micro-object is assumed to be a cylinder. First, the movement jaw does not contact the gripped micro-object, neither the gripping force nor the strain angle of flexible hinge H_3 occurs. At this time, the displacement direction of d_G and d_P is parallel, γ denotes the original distance between the movement jaw and the micro-object, as shown in Fig. 5(a). Then when the movement jaw initially contacts the micro-object, the gripping force f_G and the strain angle of flexible hinge H_3 are still zero, the output displacement of movement jaw $d_G = \gamma$, as shown in Fig. 5(b). Finally, the parallelogram mechanism continues going forward with the increase of SPCA input, however, the movement jaw is prevented by the clamped micro-object. Therefore, d_P is gradually greater than d_G ($\delta = d_P - d_G$) and the movement jaw rotates around the central axis of flexible hinge H_3, as shown in Fig. 5(c). In this case, the clamping force f_G and the strain angle of flexible hinge H_3 appear. The micro-object is clamped tightly by the movement jaw and stationary jaw.

Based on the cantilever theory, the static model of the movement jaw describing the inherent relationship between the gripping force and strain angle of flexible hinge H_3 is established in the Eq. (6).

$$\varphi = \frac{9\pi r^{1/2}L}{2\sqrt{2}Ebt^{5/2}}f_G \tag{6}$$

where φ indicates the strain angle of flexible hinge H_3 around the central axis. r and t represent the radius and thickness of flexible hinge H_3 respectively. b indicates the width of flexible hinge H_3. L denotes the length of cantilever beam. E is the elasticity modulus of aluminum alloy.

3.3. Control strategy of the clamping manipulation

In order to clamp the micro-object firmly and safely, the gripping force and the output displacement of movement jaw should be controlled accurately. The increment PID algorithm can avoid cumulative error and response rapidly according to the feedback signals. Therefore, the increment PID algorithm is adopted to control the clamping manipulation of micro-gripper. The control strategy of micro-gripper selects the visual or force feedback signal according to the contacting condition between the gripping jaw and clamped micro-object, as shown in Fig. 6. Where γ_{ini} indicates the original distance between the micro-object and movement jaw. $\gamma(k)$ denotes the real-time distance between the micro-object and movement jaw, which is acquired by extracting the feature of movement jaw from captured microscopic-vision images. $e(k)$ is the difference between the γ_{ini} and $\gamma(k)$, k is sampling number. K_P, K_I and K_D represent the proportional, integral and derivative coefficient respectively. T_0 denotes the sampling period, T_i and T_d indicate the integral and derivative constant respectively.

$$u(k) = K_P\left[e(k) + \frac{1}{T_i}\sum_{i=0}^{k} T_0 e(k-i) + T_d\frac{e(k)-e(k-1)}{T_0}\right] \tag{7}$$

First, when the movement jaw does not contact the micro-object, the SPCA input is controlled according to the visual feedback. In this case, the clamping force $f(k) = 0$, the control variable of SPCA controller $u(k)$ is represented by the Eq. (7) according to the literature [36,37]. Then when the movement jaw contacts the micro-object, the clamping force $f(k)$ is not equal to zero. In this case, the control variable $u(k)$ is calculated according to the clamping force $f(k)$ which is measured by strain sensor affixed on the central axis of flexible hinge H_3. Finally, when the difference between the maximum allowable gripping force f_{max} (Which is determined by the material properties of clamped micro-object.) and $f(k)$ is less than the setting threshold, the "*Switch*" of clamping manipulation is turned off so as to protect the clamped micro-object.

In order to avoid the cumulative error of controlling variable, the incremental input $\Delta u(k)$ is defined to control the SPCA input, as shown in the Eq. (8). Where integral coefficient $K_I = T_0/T_i$, derivative constant $K_D = T_d/T_0$. From the Eq. (8), we can see clearly that the incremental input $\Delta u(k)$ only includes three proximate sampling value, which would effectively avoid the accumulation error. Moreover, the clamping manipulation of micro-gripper is generally slow so as to protect the clamped micro-object. Therefore, the derivative adjustment can be ignored in the control algorithm of gripping manipulation. So the increment input $\Delta u(k)$ of SPCA controller can be represented in the Eq. (9).

$$\begin{aligned}\Delta u(k) &= u(k) - u(k-1)\\ &= K_P\{e(k) - e(k-1) + K_I e(k) + K_D[e(k) - 2e(k-1) + e(k-2)]\}\end{aligned} \tag{8}$$

$$\Delta u(k) = K_P[e(k) - e(k-1) + K_I e(k)] \tag{9}$$

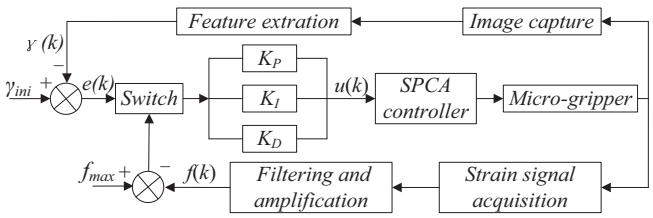

Fig. 6. Control strategy of gripping manipulation.

4. Experimental results and discussions

4.1. Experimental setup

The developed micro-gripper includes SPCA, MCM, strain sensor, SPCA cover and platform base, as shown in Fig. 7. The basic operation of micro-gripper commences by applying the desired voltage from the SPCA controller to the preloaded SPCA to activate the output motion of movement jaw. The maximum travel and motion resolution of SPCA (type: PI-P841.40) are 60 μm and 0.6 μm respectively. The MCM was made of aluminum alloy (type: 7075T6) which was very suitable for compliant mechanism due to high flexibility, and the MCM was fabricated by wire electro-discharge machining (EDM) technology. Strain sensor (type: SAK120-1-C11-P003M-V2M, Gage Factor: 2.13 ± 1%, Gage length: 1 mm, Gage Resolution: 120 ± 0.5 OHM) was sticked on the central axis of flexure hinge H_3 to measure the strain angle during the clamping process.

4.2. Verification of the kinematic model of the MCM

The experiment was performed to verify the kinematic model of the MCM established in the Eq. (5). The input displacement of the MCM was controlled by SPCA, and the corresponding output displacement of MCM could be calculated by extracting the edge of movement jaw from microscopic-vision images captured by microscopic lens (type: Navitar Zoom 6000) and CCD camera (type: AVT GC2450). Fig. 8(a) demonstrated the original position of the movement and stationary jaw. With the increase of SPCA input, the movement jaw gradually approached the stationary jaw, as shown in Fig. 8(b).

According to the geometrical parameters of the MCM listed in Table 1, the theoretical magnification ratio was calculated by the Eq. (5). In the clamping experiment, the SPCA input varied from 0 to 30 μm, the corresponding output displacement of MCM was calculated by extracting the edge of movement jaw from the microscopic-vision images. As shown in Fig. 9, the experimental and theoretical results were indicated by the red and blue lines respectively, the slope of lines denotes the magnification ratio. As shown in Fig. 9, the experimental result of amplification ratio was approximately 6.0, the theoretical result calculated by the Eq. (5) was 7.8. The theoretical magnification ratio was greater than the experimental value. The reason arising from error between the theoretical and experimental results: (1) when

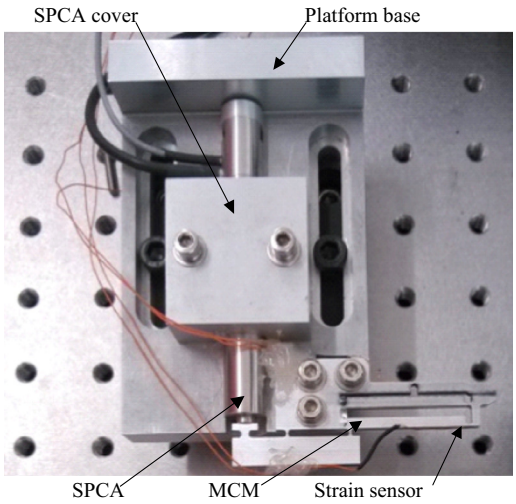

Fig. 7. The developed micro-gripper.

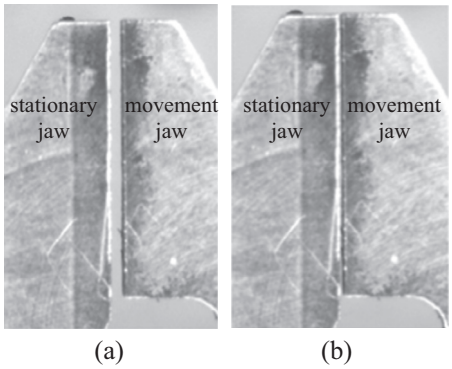

Fig. 8. The microscopic images of grasping process.

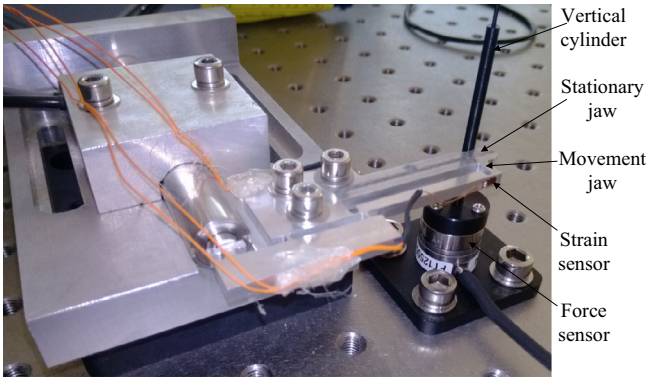

Fig. 10. The experimental setup to verify the static model.

Table 1
Geometrical parameters of the MCM.

Parameters	Value (mm)	Parameters	Value (mm)
l_1	11.75	l_4	5
l_2	14.75	l_5	30
l_3	2.75		

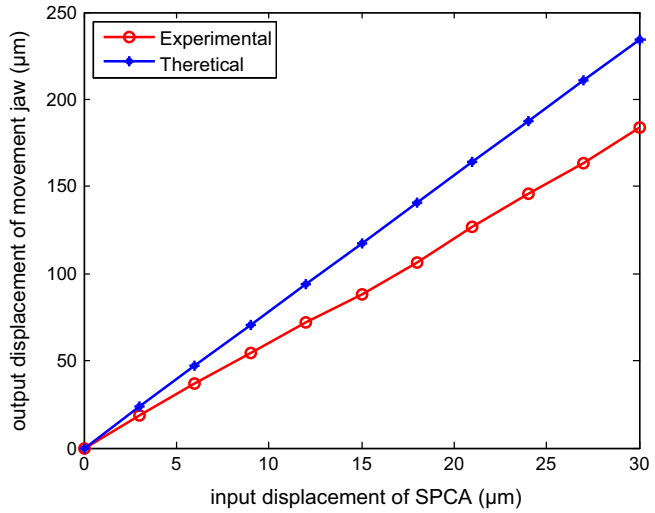

Fig. 9. Comparison of magnification ratio between experimental and theoretical results.

establishing kinematic model of the MCM, the flexible hinges are assumed to be pure bend without the expansion and contraction. However, the flexure hinges would expand and contract along their axial direction and the rotation centres of flexure hinges may deviate from the ideal position. (2) The SPCA does not lie in the central line of the MCM, which can also lead to the error between the experimental and theoretical magnification ratio.

4.3. Validation of static model of the movement jaw

The experiment to clamp the diameter of 150 μm was performed to validate the static model of the movement jaw established in the Eq. (6). The experimental setup mainly consists of force sensor, vertical cylinder, strain sensor and micro-gripper, as shown in Fig. 10. The vertical cylinder connected with the force sensor (type: ATI Nano17, sensing range: $F_x = F_y = 12$ N, $F_z = 17$ N, resolution: 3.9 mN) was in touch with the stationary jaw. When the micro-tube was clamped by the micro-gripper, the gripping force would be transmitted to the force sensor by vertical cylinder. Therefore, the gripping force between the micro-tube and movement jaw could be measured accurately. In addition, the strain angle under the gripping force was detected by the strain sensor affixed along the central axis of flexible hinge H_3. The experimental result describing the relationship between the gripping force and strain angle of flexible hinge H_3 was described in blue lines, as shown in Fig. 11. Moreover, according to the geometrical parameters of movement jaw listed in Table 2, the theoretical relationship between the gripping force and strain angle of flexible hinge H_3 was illustrated in red lines, as shown in Fig. 11.

When the strain angle of flexible hinge was less than 2×10^{-3} rad, the theoretical value of gripping force calculated from static model of the movement jaw generally tracked the experimental result, as shown in Fig. 11. When the strain angle of flexible hinge was larger than 2×10^{-3} rad, the slopes of two curves were approximately equal. Moreover, with the increase of strain angle, the variation of experimental and theoretical values is identical. Therefore, it can make a conclusion that the established static model of the movement jaw can describe the inherent relationship between the gripping force and strain angle of flexible hinge H_3. The several factors arising from the errors between the theoretical and experimental result: (1) the static model assumes the movement jaw to be a cantilever beam. When the bending angle of movement jaw under the gripping force is tiny, the assumption may be reasonable. However, with the increase of bending angle,

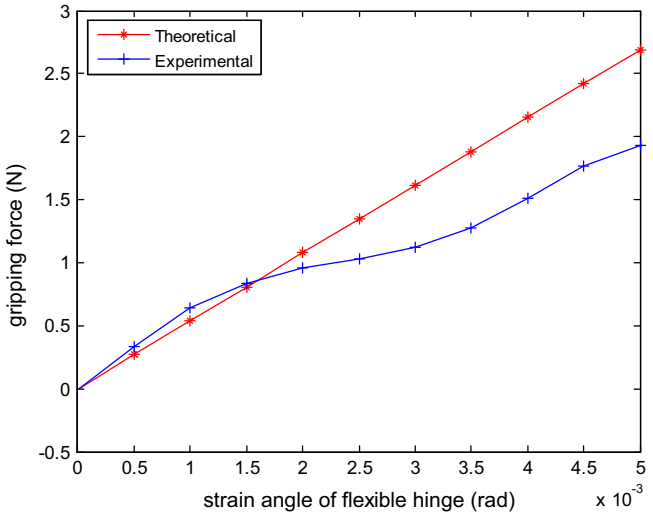

Fig. 11. Theoretical and experimental relationship between the gripping force and strain angle.

Table 2
Geometrical parameters of movement jaw.

Parameters	Value (mm)	Parameters	Value (mm)
L	7	r	1
t	0.5	b	3

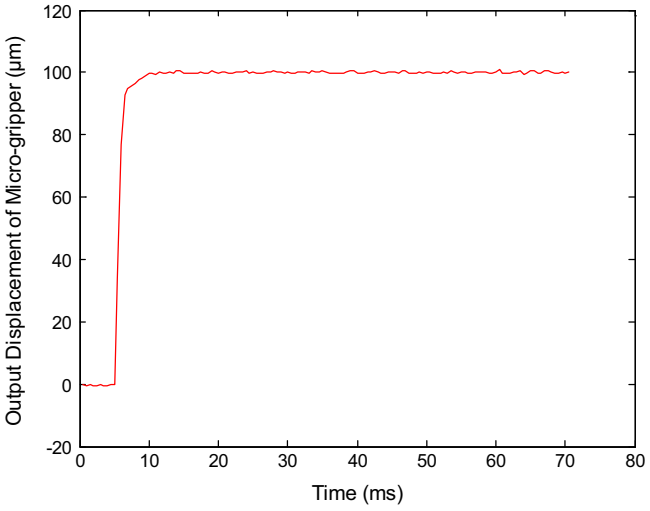

Fig. 12. The variation curve of output displacement.

the cantilever beam assumption is not suitable for the static model of movement jaw. (2) The installation of strain sensor may cause error. Ideally, the central axis of strain sensor should coincide with the axis of flexible hinge H_3 so that the strain sensor can detect the strain angle accurately. However, when the strain sensor is affixed to the flexible hinge, an angle between two axes exists inevitably. (3) The signal processing may result in the error. The signals of strain angle need to be filtered and amplified so as to perform the subsequent processing, which can cause the deviation between the theoretical and experimental values.

4.4. Characteristics of the control strategy

The control strategy of micro-gripper was verified by testing motion precision of movement jaw and stability of gripping force. First, an experiment to control the movement jaw to motion 100 μm was proposed to validate the motion accuracy of movement jaw. The input displacement of micro-gripper was controlled by SPCA, the corresponding output of movement jaw was calculated by extracting the edge of movement jaw from microscopic-vision images. According to the visual feedback acquired from microscopic-vision images, the proportional constant K_P and integral coefficient K_I were adjusted repeatedly so that the output displacement of movement jaw could be controlled accurately. Ultimately the proportional constant $K_P = 0.1$, internal coefficient $K_I = 0.8$. The experimental result was shown in Fig. 12, when the SPCA did not drive the micro-gripper, the output displacement of movement jaw initially was zero. With the increase of SPCA input, the output displacement of movement jaw reached 100 μm within 5 ms. Then the SPCA did not drive the micro-gripper further according to the control strategy. In this case, the output displacement of movement jaw remained approximately constant, the overshoot of output displacement was less than 5 μm. Therefore, based on the proposed control strategy, the motion of movement jaw could be controlled precisely and stabilized continuously, which would prevent the clamped micro-object from damaging on account of the output overshoot of movement jaw.

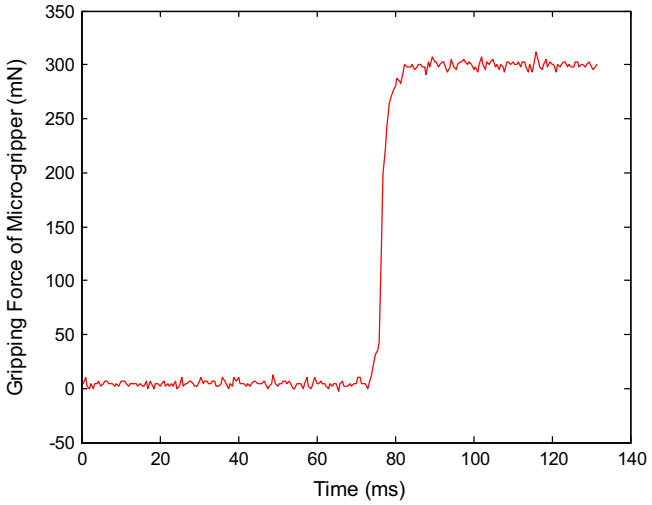

Fig. 13. The variation curve of gripping force.

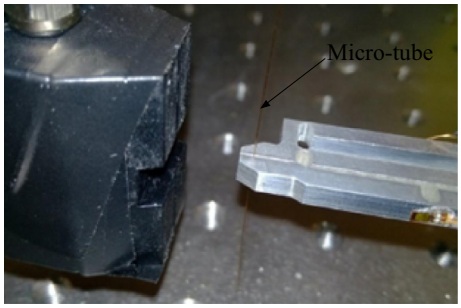

Fig. 14. The clamping manipulation of micro-tube.

Another experiment to clamp a glassy micro-tube with a diameter of 150 μm was performed to validate the stability of gripping force. In this case, the controlling goal of gripping force was 300 mN, the proportional coefficient $K_P = 0.05$, internal constant $K_I = 0.8$. The experimental result was shown in Fig. 13, the variation curve of gripping force was approximately divided into three phases. First, when the movement jaw did not contact the micro-tube, the SPCA input was controlled according to the visual feedback and the gripping force was zero. Then when the movement jaw touched the micro-tube, the SPCA input was controlled according to the feedback signals of gripping force. At this time, the gripping force reached 300 mN within 3 ms. Finally, when the gripping force reached 300 mN (the maximum allowable gripping force), the "*Switch*" of clamping manipulation was turned off to protect the clamped micro-tube. At this time, the SPCA stopped driving the MCM further, and the clamping force was stabilized at 300 mN, as shown in Fig. 13. Therefore, based on the proposed control strategy of micro-gripper, the gripping force between the movement jaw and micro-tube could be controlled precisely and stabilized continuously, which could avoid damaging the clamped micro-object due to the overshoot of gripping force. The glassy micro-tube with a diameter of 150 μm was clamped non-destructively by the developed micro-gripper, as shown in Fig. 14.

5. Conclusion and future work

This paper develops a monolithic compliant SPCA-driven micro-gripper for micro-assembly and describes the kinematic modeling, mechanism design, static model, control strategy and experimental verification of micro-gripper. The paper includes the following

points: (1) the MCM integrates the lever mechanism and parallelogram mechanism in order to amplify the SPCA input and transform the linear input of SPCA into the clamping movement of gripping jaw. The MCM adopts asymmetric structure to clamp the micro-object to improve the gripping accuracy. Moreover, the kinematic model of MCM is established to describe the relationship between the SPCA input and output displacement of gripping jaw. (2) The static model of movement jaw is established to analyze the inherent relationship between the gripping force and strain angle of flexible hinge. According to the static model, the output of gripping force can be adjusted by modifying the geometrical parameters of movement jaw. (3) The control strategy based on the incremental PID is applied to control the clamping manipulation of micro-gripper. The control strategy selects the visual or force feedback signals according to the contacting condition between the gripping jaw and clamped micro-object. The "*Switch*" of gripping manipulation is utilized to protect the clamped micro-object. Finally, a series of experiments were performed to validate the kinematic model, static model and control strategy. A glassy micro-tube with 150 μm diameter was clamped non-destructively by the developed micro-gripper. In addition, the reasons arising from error between the theoretical and experimental results have been discussed.

The experimental results have showed that: (1) the integration of lever mechanism and parallelogram mechanism can amplify the SPCA input and achieve the gripping motion. The magnification ratio of MCM calculated by kinematic model generally matches the experimental result. (2) The static model of movement jaw could reflect the relation between the gripping force and strain angle of flexible hinge H_3. (3) The control strategy of micro-gripper based on the incremental PID can satisfy with the demanding of the gripping manipulation. The motion precision of movement jaw and stable gripping force are achieved accurately.

In the future, the micro-gripper would be further explored for downsizing, and hysteresis is also considered in control strategy so as to improve the gripping manipulation. In addition, the developed micro-gripper serves as a foundation to research the dynamic response so as to obtain more robust and industrially-oriented design.

Acknowledgements

The author would like to thank the National Natural Science Foundation of China (Grant Nos. 61303177 and 61105036) which supported the development of micro-gripper.

References

[1] Bolopion A, Regnier S. A review of haptic feedback teleoperation systems for micromanipulation and microassembly. IEEE Trans Automat Sci Eng 2013;10(3):496–502.
[2] Qingsong Xu. Precision position/force interaction control of a piezoelectric multimorph microgripper for microassembly. IEEE Trans Automat Sci Eng 2013;10(3):503–14.
[3] Sharma HD, Bhardwaj S, Singh RK, Naruka GS, Tholia A. Automated alignment, focusing and control of nanomanipulators in microassembly workcell. In: International conference on mechatronics and automation; 2011. p. 177–82.
[4] Rakotondrabe M, Ivan IA. Development and force/position control of a new hybrid thermo-pieoelectric microgripper dedicated to micro-manipulation tasks. IEEE Trans Automat Sci Eng 2011;8(4):824–34.
[5] Wang DH, Yang Q, Dong HM. A monolithic compliant piezoelectric-driven microgripper: design, modeling and testing. IEEE Trans Mechatronics 2013;18(1):138–47.
[6] Komati B, Rabenorosoa K, Clevy C, Lutz P. Automated guiding task of a flexible micropart using a two-sensing-finger microgripper. IEEE Trans Automat Sci Eng 2013;10(3):515–24.
[7] Qingsong Xu. Adaptive discrete-time sliding mode impedance control of a piezoelectric microgripper. IEEE Trans Robotics 2013;29(3):663–73.
[8] Boudaoud M, Haddab Y. Modeling and optimal force control of a nonlinear electrostatic microgripper. IEEE Trans Mechatronics 2013;18(3):1130–9.
[9] Giouroudi I, Hotzendorfer H, Andrijasevic D, Ferros M, Brenner W. Design of a microgripping system with visual and force feedback for MEMS application. The Institution of Engineering and Technology Seminar on MEMS Sensors and Actuators; 2006. p. 243–50.
[10] Lopez-Wall B, Gauthier M, Chaillet N. Principle of a submerged freeze gripper for microassembly. IEEE Trans Robotics 2008;24(4):897–902.
[11] Lin Che-Min, Fan Chen-Hsien, Lan Chao-Chieh. A shape memory alloy actuated microgripper with wide handing ranges. In: IEEE/ASME international conference on advanced intelligent mechatronics; 2009. p. 12–17.
[12] Edamana B, Oldham KR. Optimal low-power piezoelectric actuator control with charge recovery for a microrobotic leg. IEEE Trans Mechatronics 2013;18(1):251–62.
[13] Zhang Yanliang, Han Mingli, Shee Cheng Yap. Calibration of piezoelectric actuator-based vision guided cell microinjection system. In: IEEE/ASME international conference on advanced intelligent mechatronics; 2008. p. 808–12.
[14] Zhou Yong, Zhou Beiyue, Li Shi. Driving performance analysis of a novel piezoelectric actuator. In: International conference on measuring technology and mechatronics automation; 2010. p. 34–7.
[15] Grossard M, Boukallel M, Chaillet N, Rotinat-Libersa C. Modeling and robust control strategy for a control optimized piezoelectric microgripper. IEEE Trans Mechatronics 2011;16(4):674–83.
[16] Grosssard M, Rotinat-Libersa C, Chaillet N, Boukallel M. Mechanical and control-oriented design of a monolithic piezoelectric microgripper using a new topological optimization method. IEEE Trans Mechatronics 2009;14(1):32–45.
[17] Nashrul Mohd, Zubir Mohd, Shirinzadeh Bijan. Development of a high precision flexure-based micro-gripper. Precision Eng 2009;33:362–70.
[18] Zubir MNM, Shirinzadeh B. Development of a high precision flexure based microgripper. Precision Eng 2009;33(4):362–70.
[19] Zubir MNM, Shirinzadeh B, Tian YL. Development of a novel flexure-based microgripper for high precision micro-object manipulation. Sensors and Actuators 2009;150(2):257–66.
[20] Nah SK, Zhong ZW. A microgripper using piezoelectric actuation for micro-object manipulation. Sensors and Actuators 2007;133:218–24.
[21] Mcpherson Timothy, Ueda Jun. Piezoelectric self-sensing technique for tweezer style end-effector. In: IEEE international conference on intelligent robots and systems; 2011. p. 1940–5.
[22] Kurita Yuichi, Sugihara Fuyuki, Ueda Jun, Ogasawara Tsukasa. Piezoelectric Tweezer-type end effector with force and displacement sensing capability. IEEE/ASME Trans Mechatron 2012;17(6):1039–48.
[23] Hideyuki Ikeda, Takeshi Morita. High-precision position using a self-sensing piezoelectric actuator control with a differential detection method. Sensors and Actuators 2011;A 170:147–55.
[24] Kawamata A, Kadota Y, Hosaka H, Morita T. Self-sensing piezoelectric actuator using permittivity detection. J Ferroelectrics 2008;368:194–201.
[25] Ivan IA, Rakotondrabe M, Lutz P, Chaillet N. Current integration force and displacement self-sensing method for cantilevered piezoelectric actuators. Rev Sci Instrum 2009;80(12):126103.
[26] Ivan IA, Rakotondrabe M, Lutz P, Chaillet N. Quasistatic displacement self-sensing method for cantilevered piezoelectric actuators. Rev Sci Instrum 2009;80(6):065102.
[27] Rakotondrabe Michy, Ivan Ioan Alexandru, Khadraoui Sofiane, Lutz Philippe, Chaillet Nicolas. Simultaneous displacement/force self-sensing in piezoelectric actuators and applications to robust control. IEEE/ASME Trans Mechatron 2012;17(6):1039–48.
[28] Xu Qingsong. A new compliant microgripper with integrated position and force sensing. In: IEEE/ASME International Conference on Advanced Intelligent Mechatronics; 2013: p. 591–6.
[29] Carrozza MC, Eisinberg A, Menciassi A, Campolo D. Towards a force-controlled microgripper for assembling biomedical microdevices. J Micromech Microeng 2000;10:271–6.
[30] Kemper M. Development of a tactile low-cost microgripper with integrated force sensor. In: International Conference on Control Application; 2004. p. 1461–6.
[31] Chang Ren Jung, Cheng Chih Yi. Vision-based compliant-joint polymer force sensor integrated with microgripper for measuring gripping force. In: International conference on advance intelligent mechatronics; 2009. p. 18–23.
[32] Beyeler F, Neild A, Oberti S. Monolithically fabricated microgripper with integrated force sensor for manipulating microobjects and biological cells aligned in an ultrasonic field. IEEE/ASME J Microelectromech Syst 2007;16(1):7–15.
[33] Jayaram K, Joshi SS. Development of a flexible-based force sensing microgripper for micro-object manipulation. J Microelectromech Syst 2010;20(1):15–25.
[34] Zubir Mohd, Nashrul Mohd, Shirinzadeh B. Development of a compliant-based microgripper for microassembly. In: IEEE/ASME international conference on mechatronic and embedded systems and applications; 2008. p. 522–7.
[35] Xuefeng Yang, Wei Li, Yuqiao Wang, Gao Ye. Output displacement analysis for compliant single parallel four-bar mechanism. In: International conference on mechatronics and automation; 2010. p. 1354–7.
[36] Widyotriatmo A, Rauzanfiqr S K, Suprijanto S. A modified PID algorithm for dynamic control of an automatic wheelchair. In: IEEE conference on control system and industrial information; 2012. p. 64–8.
[37] Tzafestas S, Papanikolopoulos NP. Incremental fuzzy expert PID control. IEEE Trans Ind Electron 1990;37(5):365–71.